CLAS-NOTE-91-007
CEBAF TN-91-022

Dispersion in Commonly Used Cables

E.S. SMITH
APRIL 11, 1991

This note describes the dispersion of fast pulses as they propagate down a variety of commonly used cables. We apply the formalism used by Fidecaro more than thirty years ago [1] to model the transmission in coaxial cables. The method, however, may be extended to ribbon cables which are routinely used to carry wire chamber signals. Here the transmission line characteristics of the cable are relatively poor, but may be modeled in a similar fashion. In the first section we introduce the framework for computation. In the second section we compare the prediction of the programs with measured distortion in a variety of cables. The final section describes the application of the formalism to a few specific cases of interest.

1 Formalism

The wave equation [2] for the voltage $V = V(z)e^{i\omega t}$, at a fixed frequency f (ω=$2\pi f$), along the length z of a coaxial line is given by

$$\frac{\delta^2 V}{\delta z^2} = \gamma^2 V, \tag{1}$$

$$where\ \gamma = \alpha + ik = \sqrt{(R + i\omega L)(G + i\omega C)} \tag{2}$$

The variables R, L, C have their usual meanings of resistance, inductance and capacitance per unit length of cable. G is the conductance per unit length of the dielectric. We also define the characteristic impedance Z of the cable

$$Z = \sqrt{\frac{R + i\omega L}{G + i\omega C}}. \tag{3}$$

In general, α and k are both complicated functions of ω, R, G, L and C. However, at high frequencies such that $R/\omega L \ll 1$ and $G/\omega C \ll 1$, α and k

may be approximated by

$$\alpha = \frac{1}{2}\left(R\sqrt{\frac{C}{L}} + G\sqrt{\frac{L}{C}}\right) \quad (4)$$

$$k = \omega\sqrt{LC} \quad (5)$$

The solution to Equation 1 is given by

$$V(z,t) = V_\omega \exp(i\omega t - ikz - \alpha z) \quad (6)$$

The explicit ω dependence of α and k is not important for the distortion or attenuation of pulses at high frequencies. The term (ikz) in the exponent gives the overall delay of the signal incurred in transmission down the cable. However, at high frequencies the resistance of the conductor, R, and the conductance of the dielectric, G (see Equation 4), may no longer be regarded as constants. It is their implicit ω dependence which gives rise to the distortion of pulses. We parametrize α in the following way:

$$\alpha = c_1 + c_2\sqrt{2if} + c_3 f \quad (7)$$

$$c_1 = \frac{R_{dc}}{2Z} \quad (8)$$

The first term corresponds to the direct current (d.c.) resistance of the center conductor. [1] The constants c_2 and c_3 were obtained as fits to the attenuation of each cable, as specified by the manufacturer in decibels per 100 m:

$$\Re(\alpha) = \left(\frac{\ln 10}{20}\right) \times Attenuation(dB) \quad (9)$$

The parametrization of α for several cables in shown in Figure 1 and the constants are listed in Table 1. The second term represents the frequency dependence of the resistance through the *skin effect*, which has equal real and imaginary parts. The third term is due to leakage across the dielectric and models the frequency behavior of G. A quick glance at the table shows

[1] The resistance of the shield may also contribute to R_{dc}. However, in general this depends on the specific cabling scheme and in practice if R_{dc} is important the shield resistance may be neglected.

Table 1: Constants used to specify the behavior of α for several cables of interest. The real part of α was fitted to the form $c_1+c_2\sqrt{f}+c_3$f, with the frequency expressed in MHz and the constants in units of $(100\ \mathrm{m})^{-1}$. The first constant is determined by the d.c. resistance of the cable conductor.

Description	Cable Type	c_1	c_2	c_3
Flat Ribbon Cable [2]	9V28	.107	.581	.0084
Ribbon Coaxial Cable [2]	9K50	.239	.385	.0000
RG-174	Belden 8216	.320	.259	.0028
RG-58	Belden 8259	.035	.144	.0036
RG-213	Belden 8267	.006	.060	.0011
Low Loss Semi-solid Polyethylene	Belden 9913	.003	.045	.0003
Low Loss 7/8" Foam	HELIAX LDF5	.001	.013	.00001

that by far the most important term is c_2, but in the limits of low (high) frequency c_1 (c_3) cannot be ignored.

A voltage pulse may be represented by a Fourier Integral as

$$V(z,t) = \frac{1}{2\pi}\int_{-\infty}^{+\infty} V_\omega \exp(i\omega t - \alpha z)d\omega \tag{10}$$

$$V_\omega = \int_{-\infty}^{+\infty} V(0,t)\exp(-i\omega t)dt \tag{11}$$

Here we have ignored the fixed delay in the cable, which will not affect the shape of the pulse as it travels down the cable. The shape of the pulse V(z,t) is computed at any position z along the cable by insertion of the appropriate values of α (from Equation 7) and V_ω as determined in Equation 11. In practice one must evaluate these expressions numerically with fast Fourier transform techniques [3].

[2]The specifications for this cable are given only up to 100 MHz.

1.1 Square Wave

The case of a square input pulse of width Δ, beginning at t=a, may be computed analytically using tabulated Laplace transforms. This ideal case is worth investigating since the solution may be obtained in closed form. We rewrite the above equations for V(z,t) making the substitution s=iω. We also make the simplification that c_1=c_3=0.

$$V(z,t) = \frac{1}{2\pi i}\int_{-i\infty}^{+i\infty} V_s \exp(st - c_2\sqrt{\frac{s}{\pi}}z)ds \tag{12}$$

$$V_s = \frac{e^{-as}(1-e^{-\Delta s})}{s} \tag{13}$$

$$V(z,t) = Erfc\left(\frac{1}{2\sqrt{\frac{(t-a)}{\tau_0}}}\right), \qquad a \leq t \leq a+\Delta \tag{14}$$

$$= Erfc\left(\frac{1}{2\sqrt{\frac{(t-a)}{\tau_0}}}\right) - Erfc\left(\frac{1}{2\sqrt{\frac{(t-a-\Delta)}{\tau_0}}}\right), \qquad t \geq a+\Delta$$

Erfc(x) is the complementary error function defined in the standard way. Causality imposes that the voltage signal V(z,t) be zero before t=a. The term c_1, if included, will contribute an overall factor of $e^{-c_1 z}$. The rise time of the signal is determined by the parameter

$$\tau_0 = c_2^2 z^2/\pi \quad (\mu s) \tag{15}$$

We note that τ_0 and therefore the dispersion increases as the square of the constant c_2 and the length of cable z. This relation may be used to scale results from one cable to another when c_1 and c_3 can be neglected.

In Figure 2 we compare the analytical formula given by Equation 14 with the numerical transforms using Equations 10 and 11. The conditions are such that c_1 and c_3 are small, so the agreement is good. We note some technical difficulties encountered when using numerical transforms at sharp boundaries which show up as oscillations in the beginning and the end of the square pulse in Figure 2. (See also Figure 5). Improved accuracies may be achieved by

increasing the sampling grid for the transform. For many applications these numerical problems are minimal because in practice pulses have finite rise times [6].

2 Comparisons with data

We have measured the response of several coaxial cables to a NIM logic signal (−.75 V and of 10 ns duration). These include RG-58, standard cable for fast NIM electronics, RG-213, formerly RG-8A/U and Belden 9913, a low-loss semi-solid polyethylene cable. The lengths of the cables ($\sim$ 300 ns) were chosen to match the time required to form a first level trigger for the CLAS detector [4]. The shapes of the signals, shown in Figure 3, are well-reproduced including the leading and falling edges. Note that the cable dispersion in high quality Belden 9913 is approximately equal to the dispersion in standard RG-213 cable for the same time delay. This is due to the fact that the slower velocity in RG-213 (β=.66 vs β = .84 for 9913) compensates for the larger attenuation as a function of cable length (see constant c_2 in Table 1). Thus, either cable serves equally well for the purpose of delaying signals. The dispersion in RG-58 is so large that after 80 m of cable, the original logic signal must be regenerated.

The response of RG-174, miniature cable used for short cable connections, was measured in response to a NIM signal of 50 ns duration in order to allow the output signal approach its asymptotic level (see Figure 4). This level corresponds to low Fourier frequency components and the d.c. resistance becomes important (see Equation 8). However, given that approximations were made which are only valid in the high frequency regime, one should not expect the low frequency limit to be reliable. However, it is worth investigating this limit, as it is important in some practical applications. For example, ECL logic signals are often transmitted over long distances using flat ribbon cable. In the d.c. limit the voltage levels are reduced by

$$\frac{V_{out}}{V_{in}} = \frac{1}{1+\frac{R}{Z}} \simeq 1 - \frac{R}{Z}. \tag{16}$$

This is twice the value expected in lowest order from Equation 8. To illustrate the effect of the term c_1, consider the result of the simulation in Figure 5 for the propagation of a 1μs logic pulse through 100 m of RG-174 cable. The

simulation also shows the output pulses expected for the case when c_1=0. The voltage level expected in the d.c. limit is 0.44 V. The simulation gives 0.5 V, somewhat lower than that from using the term c_1 alone (0.55 V), and closer to the actual value. However, neglecting this term altogether has a dramatic effect in this limit, as shown in the Figure, and cannot be ignored.

A final comparison with data was made for the response of twisted-pair flat ribbon cable (Belden 9V28) to a fast analog signal coming from the CLAS [4] drift chamber pre-amplifier (see Figure 6). This study was undertaken to consider the possibility of carrying these signals through 30 ft (9.14 m) of ribbon cable from the pre-amplifier, situated next to the drift chamber wires, to the post-amplifier located in electronic racks outside the detector system. The simulation predicts that the signal would be attenuated by 0.6 compared to the measured value of 0.7. However, the rise and fall times of the pulse are well reproduced.

3 Applications

The dispersion of an Amperex XP2262 photomultiplier (PMT) pulse after 50 m of RG-213, RG-58 and RG-174 is shown in Figure 7. The pulse shape is retained by the RG-213 cable and slowly deteriorates for RG-58 and RG-174. The increase in rise time with cable length is relatively slow relative to the expectation given by Equation 15. This can be traced to the very narrow pulse width of the photomultiplier. For wider pulses, the rise time is no longer limited by the pulse width and degrades faster with increasing cable length. This is illustrated in Figure 8 which shows the rise times as a function of cable length for two pulses of different widths. The time slewing of the pulse with pulse height for the photomultiplier pulse is shown in Figure 9 for various cable lengths. The magnitude of the time-walk increases for the longer cable lengths as expected, roughly in inverse proportion to the rise time. The slewing of the time measured by a leading-edge discriminator as the pulse height is varied by $\pm$50% is 1.15 ns for the pulse directly out of the photomultiplier compared to 1.45 ns after the pulse is delayed by 100 m of RG-213 cable. Estimates for other cables may be obtained by use of Equation 15 in the approximation that c_1 and c_3 are neglected.

As pulses propagate down a cable, they disperse over time and narrow gates may no longer contain the total charge. This effect is illustrated in

Figure 10. A PMT pulse with a baseline width of 30 ns is totally contained inside a 40 ns gate. However, only 85% of the charge is inside the gate after 50 m of RG-58 cable. After 100 m of RG-213 cable 88% of the signal is still inside the gate. The long tails will also cause a change in the d.c. baseline at high rates which will be shifted by the average charge injected onto the cable.

In a final example (Figure 11) we show the accelerator RF timing signals (500 MHz) which control the CEBAF beam structure to each End Station. The control signals are carried by low-loss 7/8" foam cable. After a 1000 ft run of cable the sine waves are attenuated by a factor of two. Because the input is a pure sine wave the output signal is not distorted, simply shifted in phase.

ACKNOWLEDGEMENTS

I would like to thank Amrit Yegneswaran for providing measurements of dispersion in flat ribbon cable. I also wish to thank Fernando Barbosa and Don Joyce for useful discussions and suggestions to improve original drafts of this paper.

A Program WAVE_PROP

We describe the implementation of the numerical evaluation of pulse dispersion in the program WAVE_PROP. WAVE_PROP is written in FORTRAN and adapted to allow the user to select a variety of pulse shapes and display the expected output from a number of commonly used cables after a specified length. The Fourier transforms are evaluated using the real fast Fourier transform routine RFFT from the CERN library KERNLIB [3]. For ease of implementation and portability, the source code for this routine is available with the source for WAVE_PROP.

WAVE_PROP has two output files. The first is a file, WAVETOP, may be used as an input the plotting program TOPDRAWER [2] [7]. It contains two plots. One shows the input and output pulses as a function of time. The other shows the time slewing of the output pulse as a function of pulse height. The second file, WAVELIST, lists all parameters which were used

[3]While it is very convenient to use TOPDRAWER to display the output plots, the files are simply columns of ASCII numbers which may easily be used either as inputs to another plotting package or for any other application.

during the program as well as a few key parameters of the input and output pulses.

The input file to WAVE_PROP contains the information to select the type of pulses and cable combinations one wishes to study. A sample procedure to run the program which includes the input file may be found in the file WAVE_PROP.BAT. In the following each input line is described in detail.

1. Computation Period

   The numerical computation of Fourier integrals can only be achieved over finite intervals. In practice this has the effect of modeling a repetitive signal with a period given by this parameter. Internally the program samples this interval 256 times which determines the maximum Fourier frequencies used. Pileup effects are visible in the output when the tails of the output spill over into the next period.

   Format :
   Period

2. Input pulse specification

   Name of pulse specification and two parameters specifying the pulse. The following is a list of values accepted by the program. Only the parameters which are relevant to a given input are specified. Unused parameters will nevertheless be read by the input file. Units of time are ns and frequency is MHz.

   - 'DC' – digitized drift chamber calibration pulse.
   - 'PMT' – digitized Amperex XP2262 PMT pulse.
   - 'GAUSS', mean, sigma – Gaussian function.
   - 'SINE', frequency, phase – Sine function.
   - 'PULSE', peak, a – function $t^a \exp(-bt)$, peak=a/b.
   - 'STEP', width – square wave.
   - 'NIM', width – digitized output from a standard NIM logic discriminator.

Format :
'NAME', parameter, parameter

3. Title for TOPDRAWER plots

   String with the title for the TOPDRAWER plots.

   Format :
   'TITLE'

4. Case specification for TOPDRAWER plots.

   String which interprets the TOPDRAWER title string. This allows the use of upper and lower case, Greek, superscripts and subscripts, etc. [7].

   Format :
   'CASE'

5. Limits for abscissa of first TOPDRAWER plot.

   The integrated value of the pulse given in the list file is the charge collected during this interval.

   Format :
   Low limit for x-axis, High limit for x-axis

6. Number of cables used.

   For each cable used, one line specifying the cable and its length must follow.

   Format :
   Number

7. Cable type, length

   A string specifying the cable type, followed by the length of the cable. The cables types currently implemented are:

- '9V28' : Belden catalog p. 183, .050 Vari-Twist Flat Cable (28 gauge).
- '9VK50' : Belden catalog p. 185, 50 ohm Ribbon Coaxial Cable (28 gauge).
- 'RG174' : RG-174, Belden 8216.
- 'RG58' : RG-58, Belden 8259.
- 'RG213' : RG-213, formerly RG-8A/U, Belden 8267.
- '9913' : Low loss semi-solid polyethylene RG-8, Belden 9913.
- 'LDF5' : Low loss 7/8" foam, HELIAX LDF5.

Format :
'TYPE', length in meters

8. Discriminator Threshold.

   Discriminator threshold used to compute the time slewing which is plotted in the second TOPDRAWER figure. The threshold is expressed as a fraction of the peak value of the output pulse.

   Format :
   Threshold

9. Limits of abscissa on second plot.

   The limits are given as a multiplier of the nominal output pulse height value. For example [.5,1.5] will plot the time slewing when the output pulse varies from half to one and a half times its computed value.

   Format :
   Low limit for y axis, High limit for x-axis

10. Limits of coordinate axis on second plot.

The y-axis gives the time at which the output pulse crosses the threshold for the range of input pulse height variations given by the abscissa limits.

Format :

Low limit for y-axis, High limit for y-axis

References

[1] G. Fidecaro, Nuov. Cim. suppl. to Vol. **15**, Series X, 254 (1960).

[2] W.R. Leo, *Techniques for Nuclear and Particle Physics Experiments*, Chapter 13, Springer-Verlag, 1987.

[3] We used the routine RFFT (D703) from the CERN Program Library KERNLIB. We found that the dimensionality of the space used by the transform, $n=2^8$, to be adequate for our needs.

[4] "Conceptual Design Report — Basic Experimental Equipment," CEBAF April 13, 1990.

[5] Belden Wire and Cable, Master Catalog, P.O. Box 1980, Richmond, IN 47375.

[6] Finite Fourier transforms are widely discussed. See for example chapter 5 in H. Joseph Weaver, *Applications of Discrete and Continuous Fourier Analysis*, John Wiley & Sons, New York, 1983.

[7] Roger B. Chaffee, *Top Drawer Manual*, SLAC Computation Group.

List of Figures

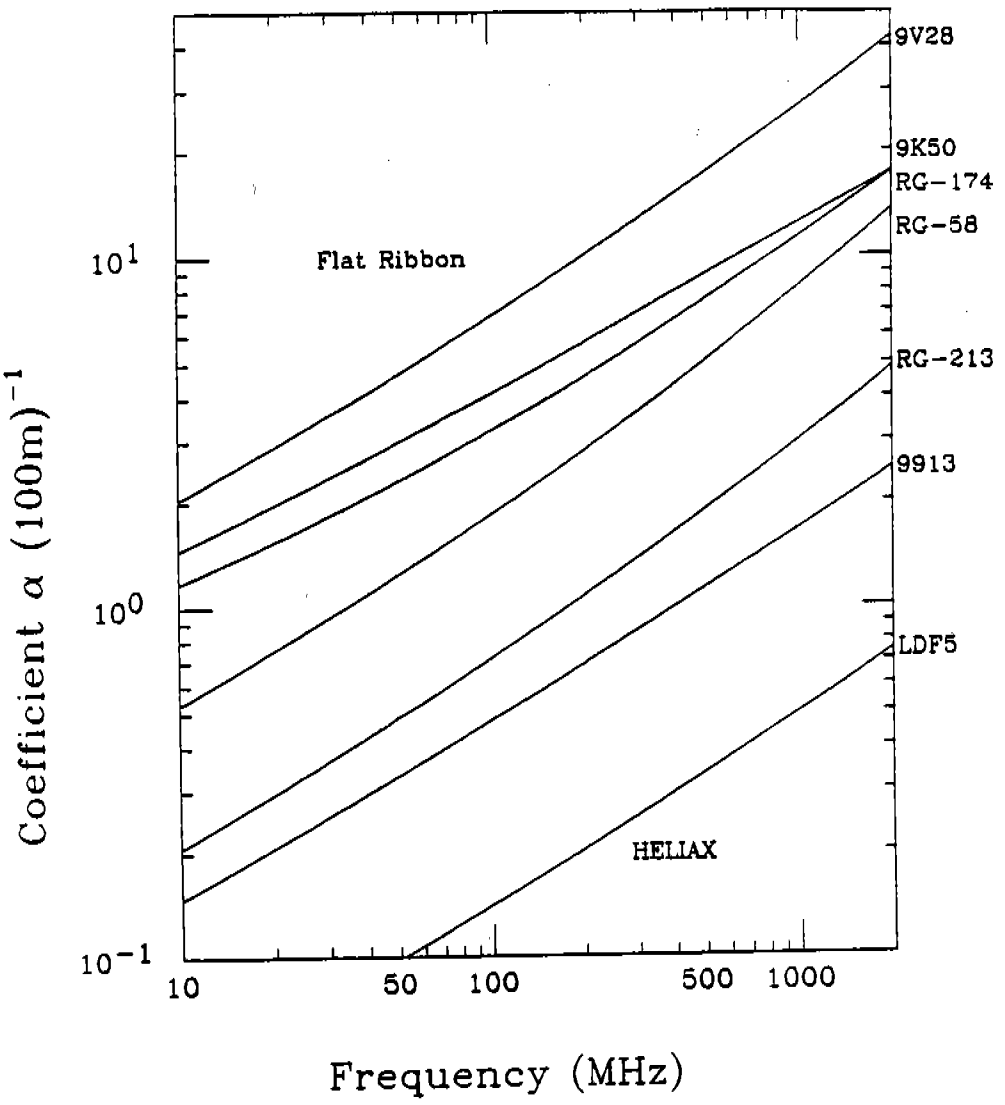

Figure 1: The dependence of the attenuation coefficient on frequency for cables ranging from flat ribbon cable through 7/8" foam HELIAX.

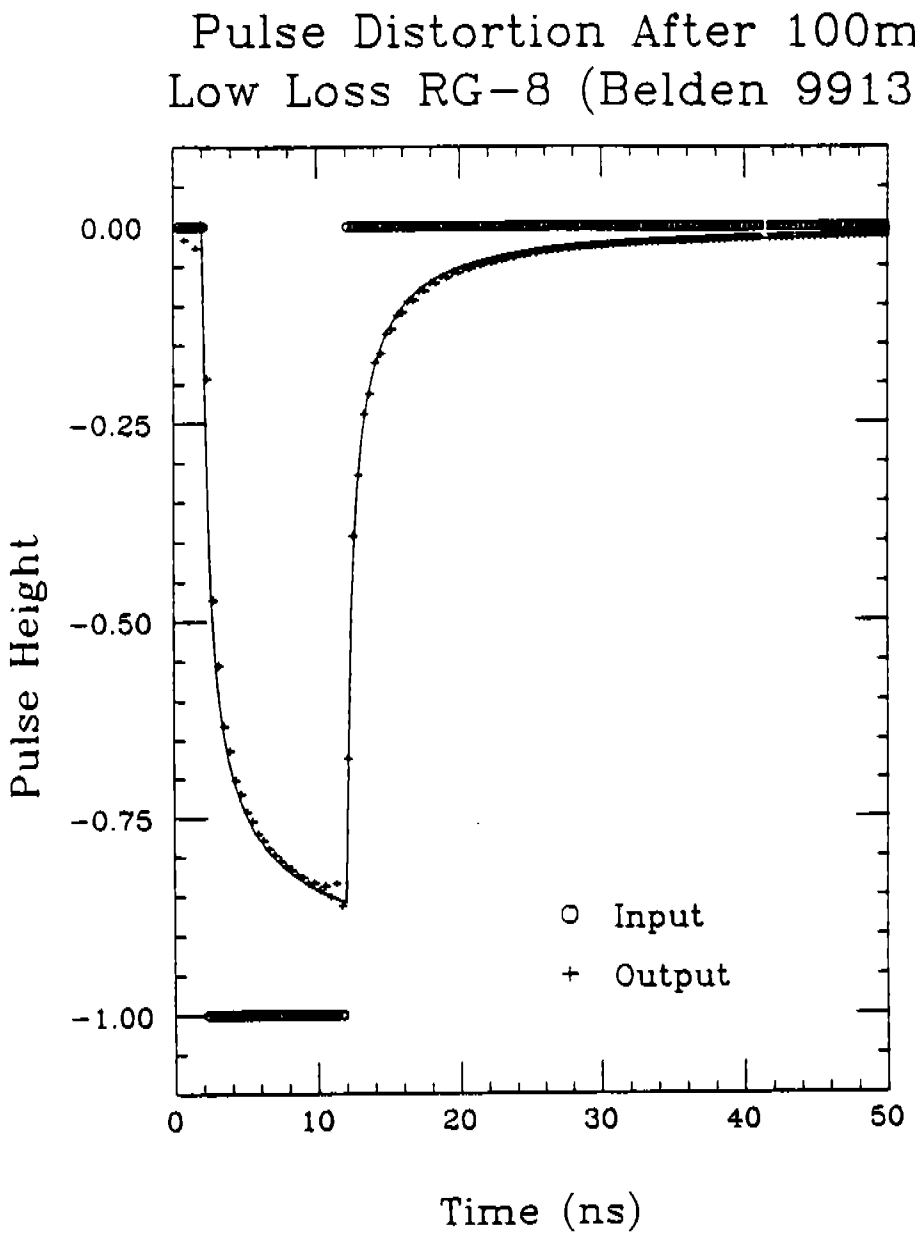

Figure 2: Comparison of numerical and analytical results for a square wave. Oscillations of the numerical computation near the leading and trailing edges of the pulse are due to the restriction to a finite number of frequencies in the Fourier transform.

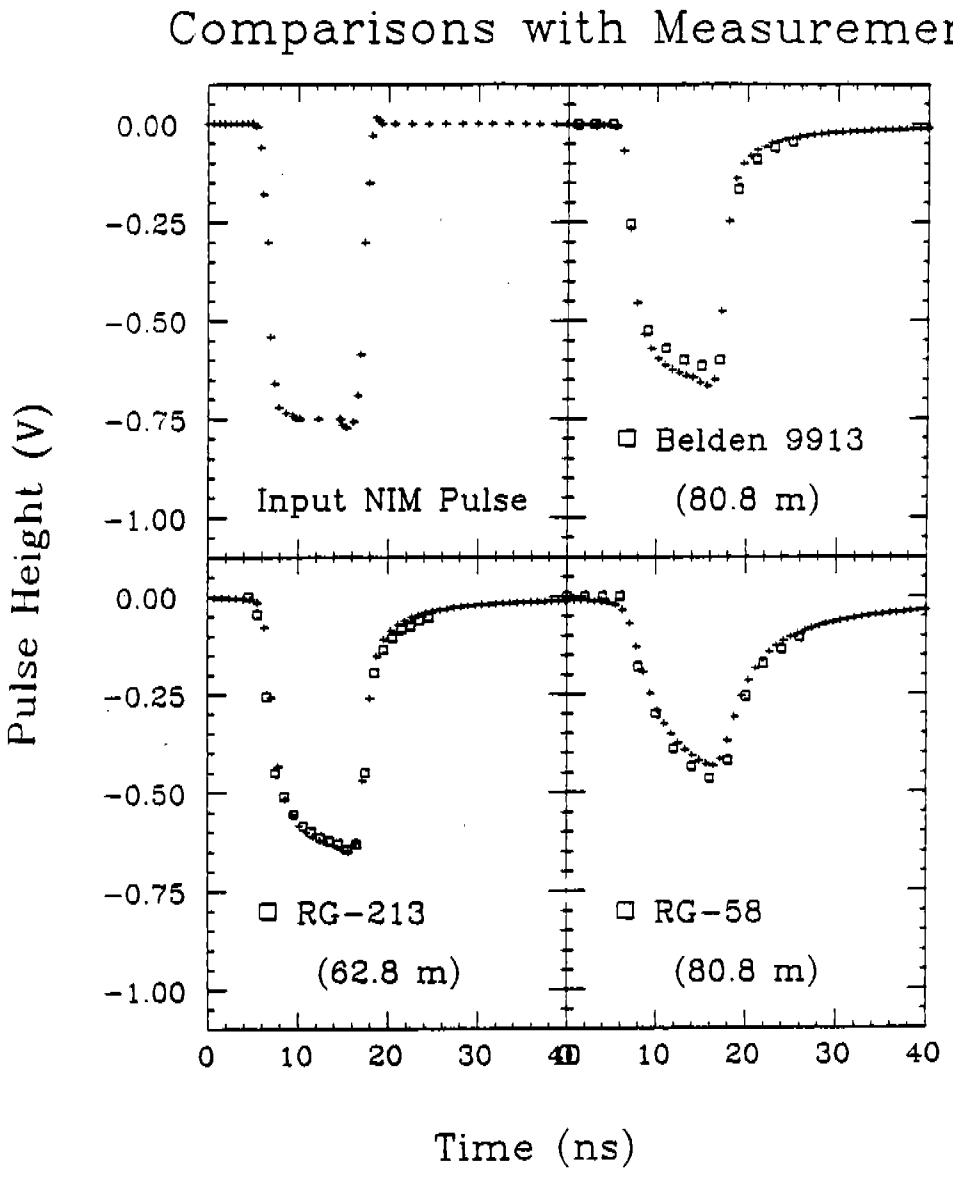

Figure 3: Comparison of the simulation with measurements for three coaxial cables. The input pulse is a standard NIM logic signal 10 ns wide.

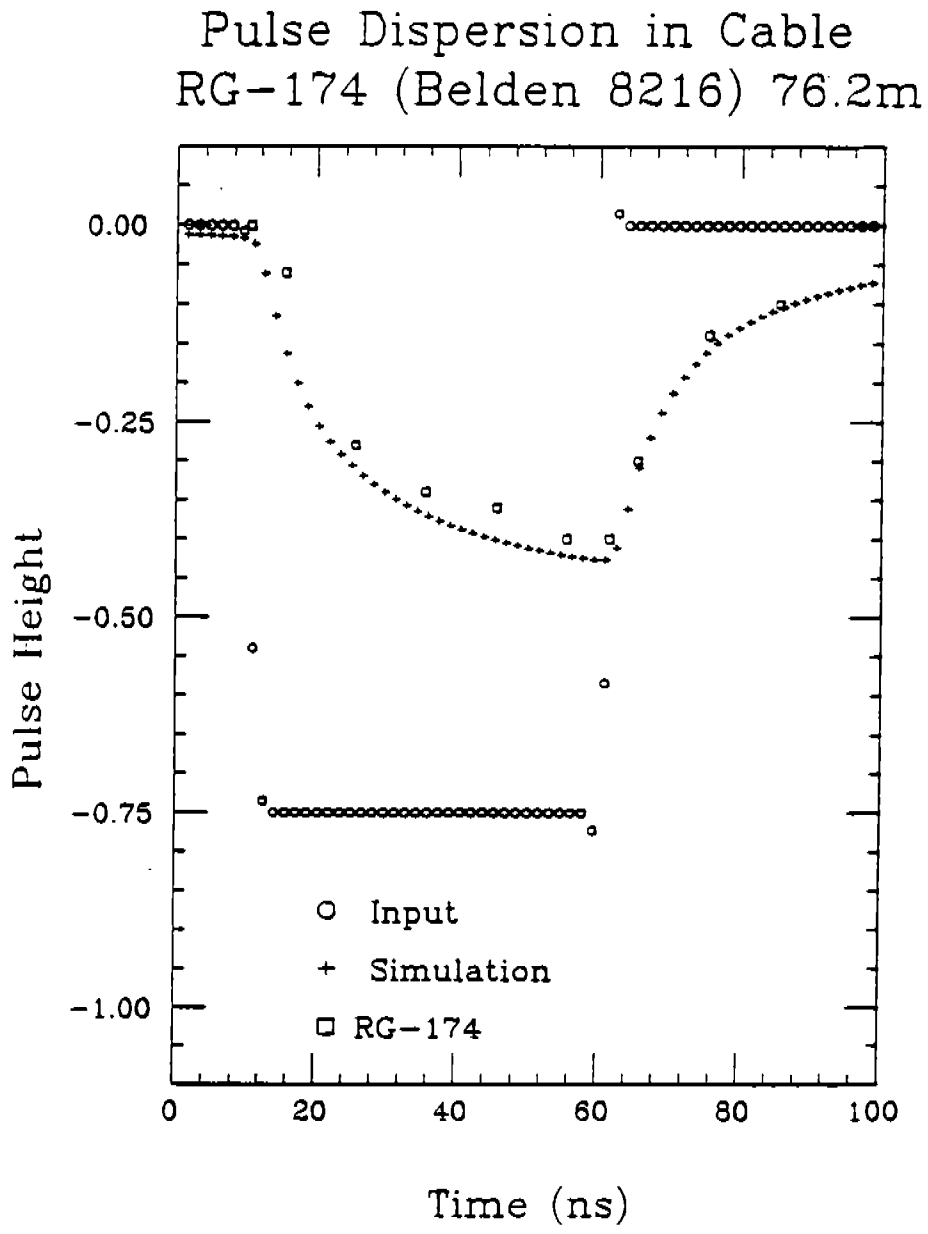

Figure 4: Comparison of the simulation with measurements of a standard NIM logic signal (50 ns wide) after propagation through 72.6 m of RG-174 cable.

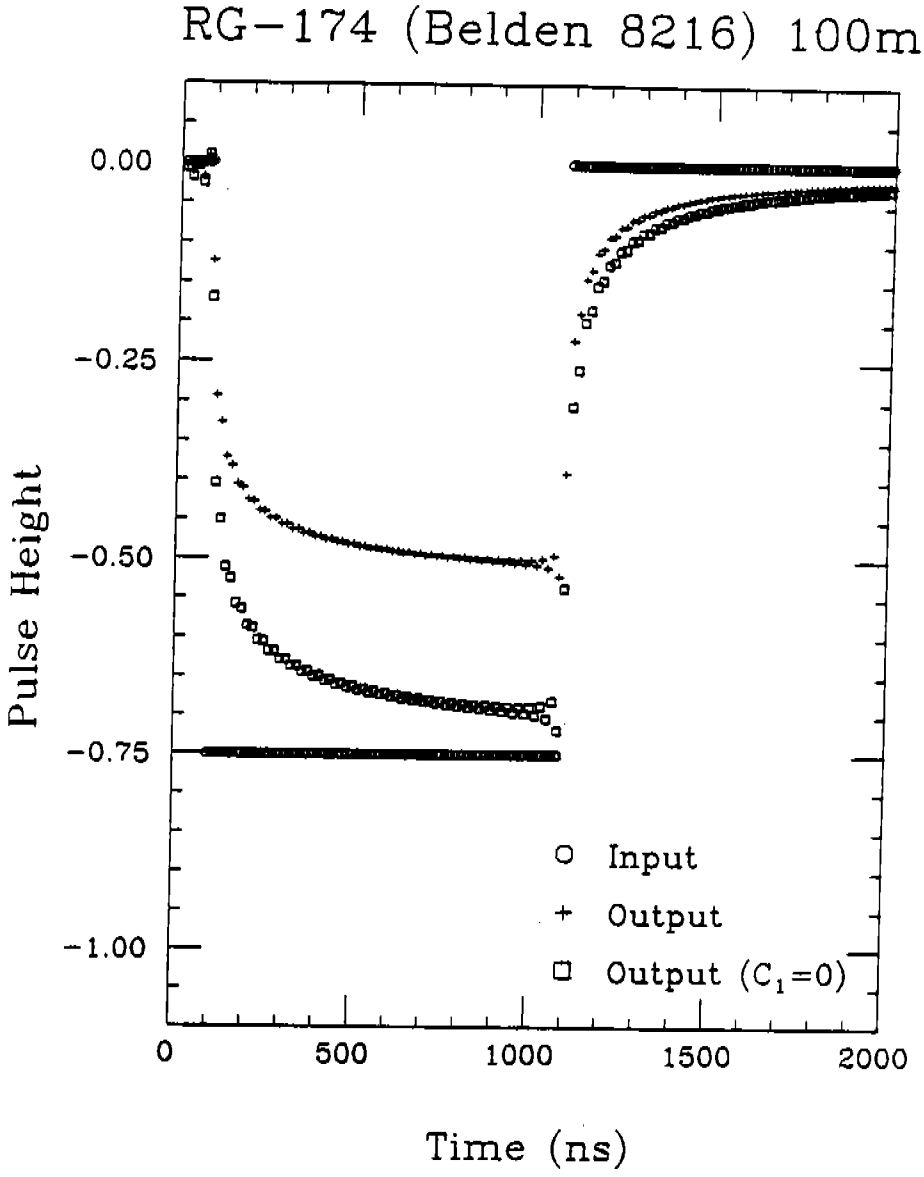

Figure 5: The role of the d.c. resistance (c_1) is demonstrated here in the final level achieved by a very long pulse. Oscillations of the numerical computation near the leading and trailing edges of the pulse are due to the restriction to a finite number of frequencies in the Fourier transform.

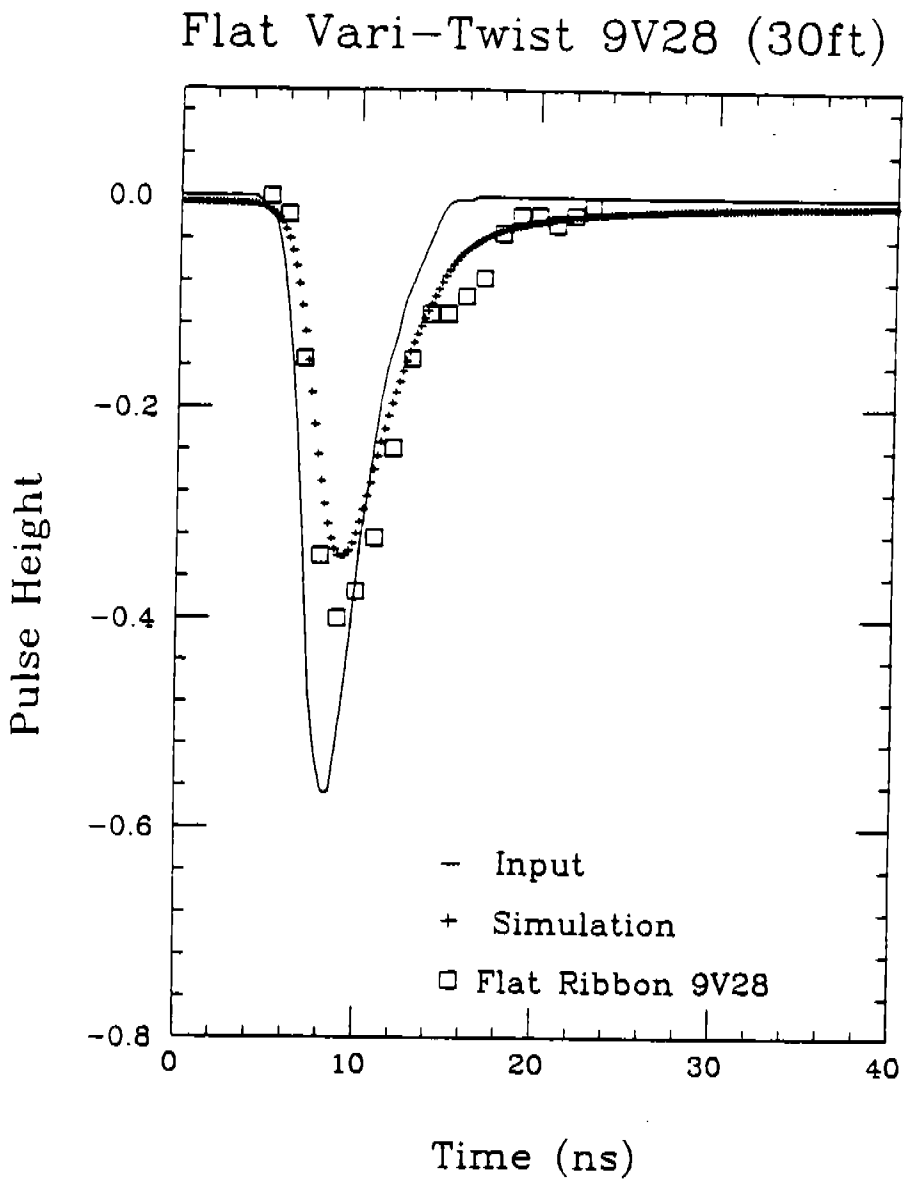

Figure 6: Comparison of the simulation with measurements for a drift chamber calibration pulse after propagation through 30 ft of flat ribbon cable.

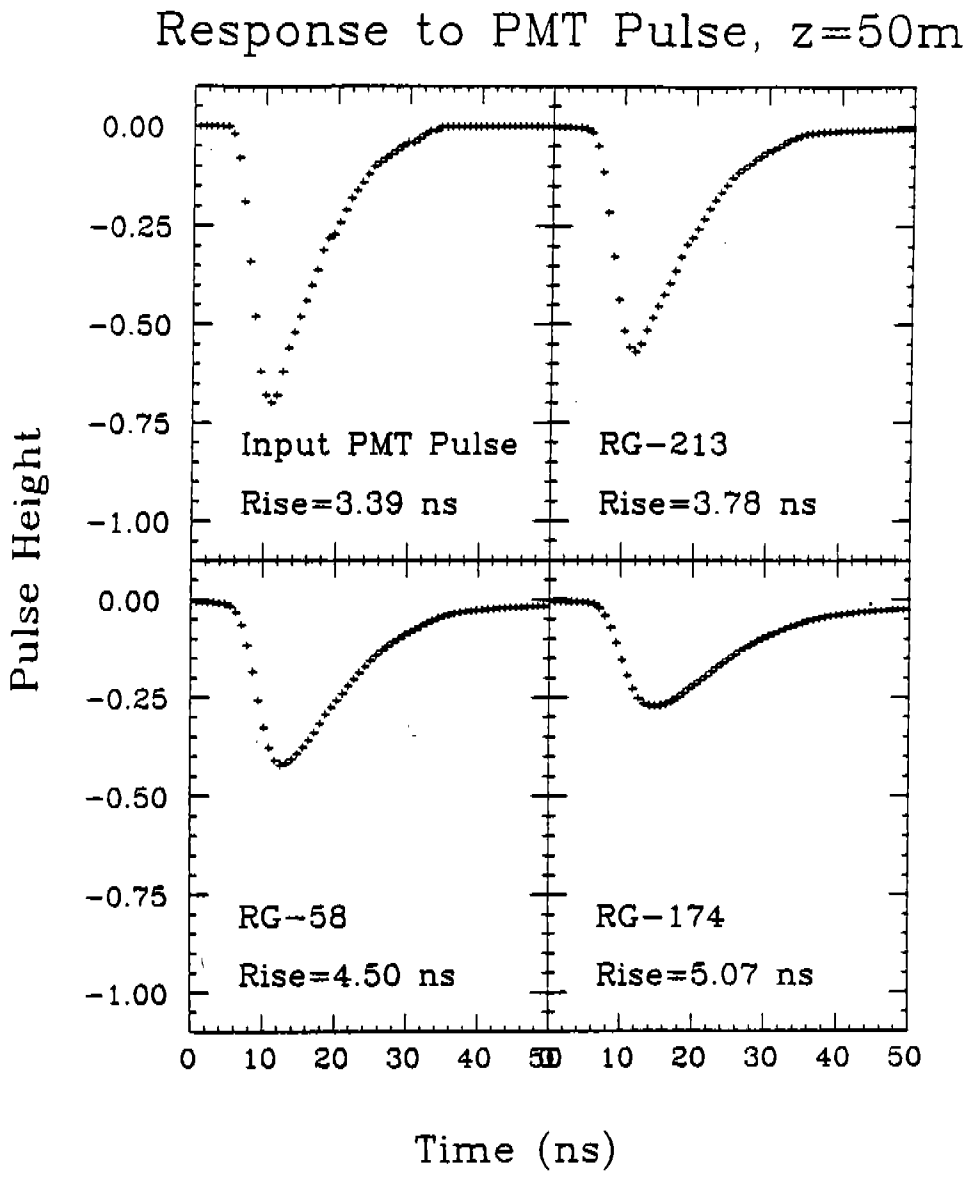

Figure 7: The simulated response of three coaxial cables is shown to a fast PMT signal. The rise time increases only slightly because the input signal is so narrow.

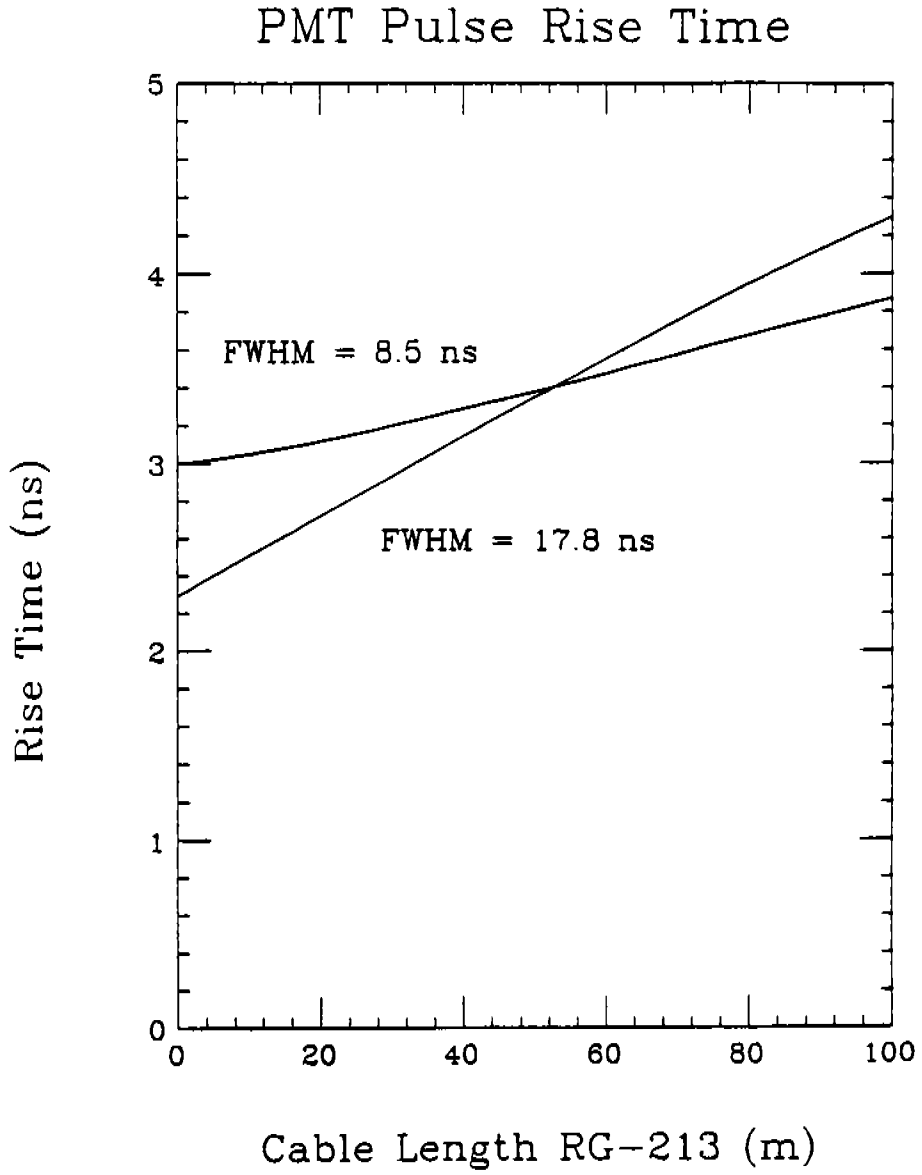

Figure 8: The rise time of two fast signals increases as the signal propagates down RG-213 cable. For very narrow pulses, the rise time does not deteriorate as fast as it does for wide pulses.

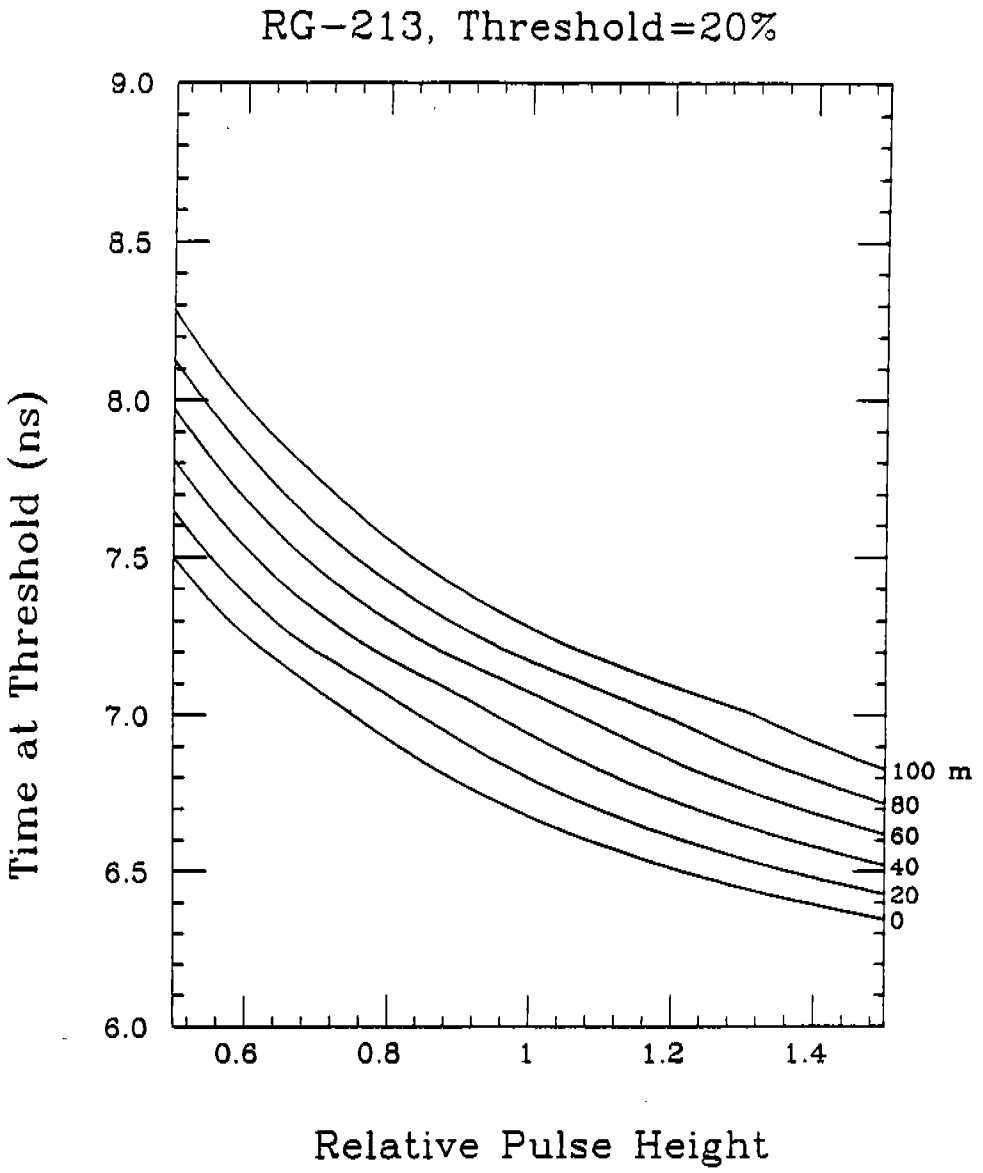

Figure 9: The time slewing for various cable lengths of RG-213 (scale on right). The time is plotted for a leading-edge discriminator at 20% of the nominal output pulse height (one in relative units) for that length of cable.

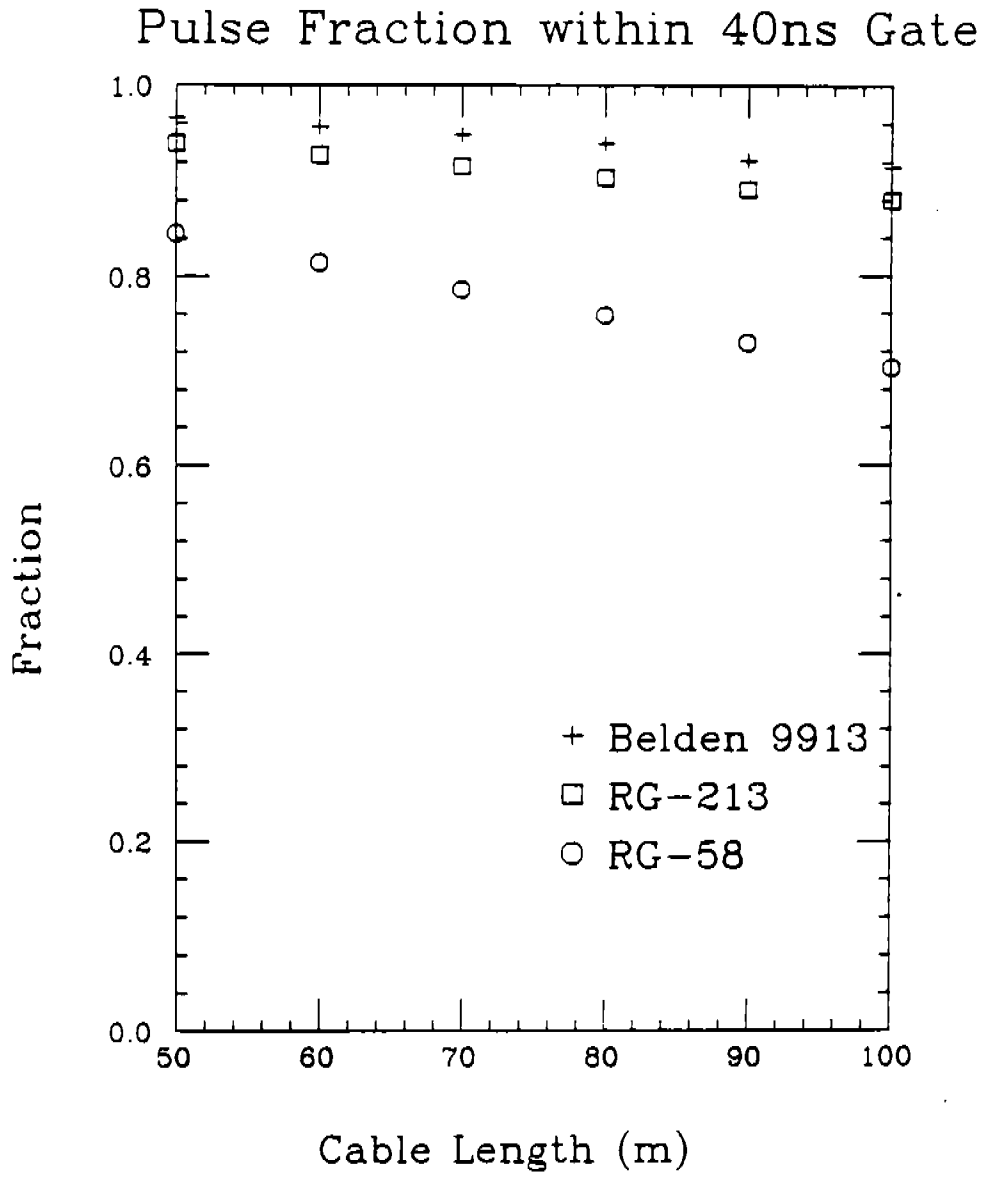

Figure 10: The fraction of charge of a fast pulse (30 ns at the baseline) contained within a 40 ns gate is plotted for three coaxial cables as a function of cable length.

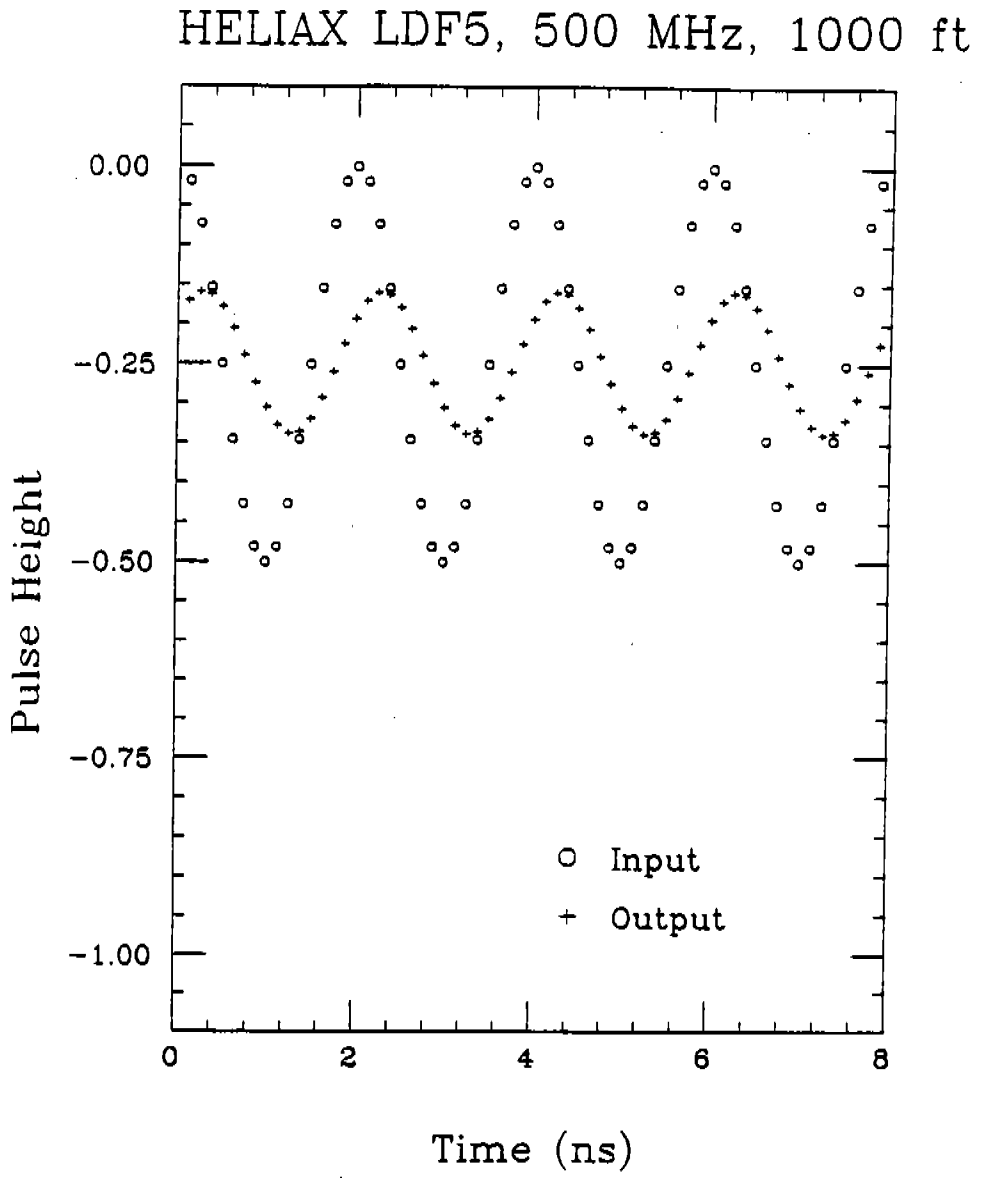

Figure 11: The output of a 500 MHz sine wave after propagation through 1000 ft of low loss 7/8" foam coaxial cable. The amplitude of the sine wave decreases by two but is not distorted.